

Chapter 5

Late Pleistocene monsoon variability

The Pleistocene epoch is known for several glacial-interglacial events and contemporaneous marine, fluvial, lacustrine deposits [*Kay, 1931*]. The Pleistocene ended with last glacial event at 11.7 ka. It is convenient to describe Pleistocene climate variability in terms of Marine Isotopic Stages (MIS) or Glacial-interglacial events. In the present study an attempt has been made to explain ISM variability during different MIS and glacial-interglacial events.

Marine isotope stages (MISs) or Oxygen isotope stages (OISs) are the alternate glacial-interglacial events marked on $\delta^{18}O$ variations observed in sediment cores from the ocean. They form the standard stratigraphic scale and are used extensively to correlate Quaternary (i.e. the last ~ 2 million years) climatic events. Seven Marine Isotopic Stages comprising of two complete glacial cycles (190-80 ka and 80 ka to present) span the past 200 ka. The Indian monsoon generally responds to interglacial/glacial events either by intensification/weakening of its strength. A majority of reconstructed monsoon records for the past 200 ka derive from marine sediment cores. They preserve the complete and continuous Quaternary monsoon records. Terrestrial records on the other hand are discontinuous, as preceding glacial evidences could be wiped out by the follow-

ing interglacial event. Although oceanic record is complete, continuous and well dated, it records the strength of the monsoon winds or ice volume rather than a direct measure of past precipitation except in the coastal regimes. Terrestrial proxies, on the other hand, record changes in monsoon precipitation. A significant amount of work has been done to reconstruct monsoon rain using aeolian, fluvial, lacustrine and peat deposits. The present study focuses on reconstructing late Pleistocene ISM variability based on a speleothem records from the Kailash and the Belum caves and a sediment core from the Andaman Sea, a literature data.

5.1 Terrestrial records

Although the oceanic record is complete, continuous and well dated, some of the proxies used record the strength of the monsoon winds rather than a direct measure of past precipitation. ISM strength is not linearly correlated with strength of wind, instead it depends upon the moisture carried by the winds depending on the SST in the southern hemisphere and rate of ascent of the parcels after they cross Indian coasts [*Rashid et al., 2007*]. Terrestrial proxies, on the other hand, record changes in monsoon precipitation. A significant amount of work has been done to reconstruct monsoon rain using aeolian, fluvial, lacustrine and peat deposits. Figure 5.1 shows such locations where extensive work has been done to reconstruct past climate. Fluvial sediments of the Sabarmati and Mahi Rivers on the southern margin of the Thar Desert are repositories of monsoon records for past 130 ka. Enhanced monsoon conditions during the MIS 5 (sub-stages e, c and a) interglacial period are seen as fine flood plain deposits on river banks. The cooler phases of MIS5-d(120-100ka) and MIS4 (74-60ka), when monsoon weakened, this signal is well represented by braided river facies [*Juyal et al., 2006*]. During Last Glacial Maximum (comprising MIS-2), extreme weakening of the monsoon is seen, where the fluvial sedimentation is replaced by aeolian (i.e.

wind-blown) deposition. The complete sequence was incised in the beginning of the Holocene, when monsoon regained its strength.

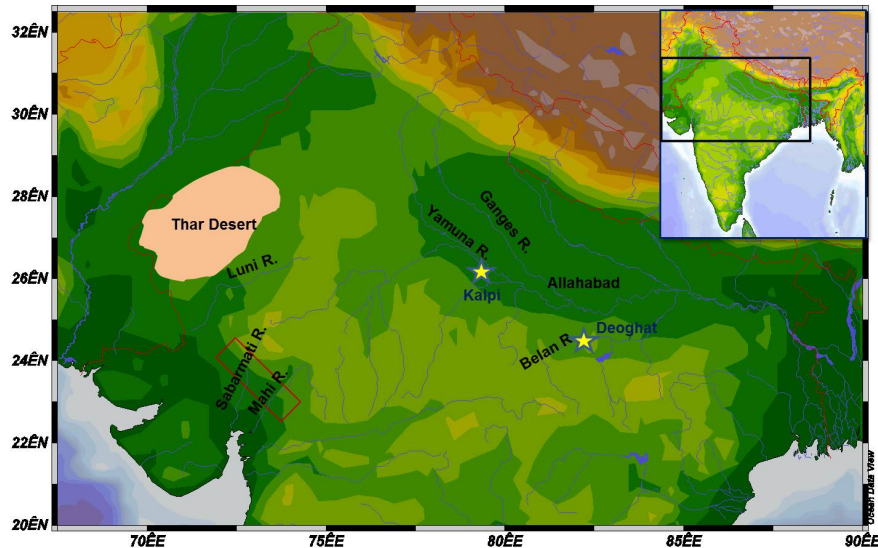


Figure 5.1: Locations of different terrestrial records from the core monsoon region of India. Image source: Ocean data viewer

Another core raised from the Luni River flowing through the Thar Desert shows that below the present aeolian sand sequence lies fluvio-aeolian deposits of the Quaternary. Sedimentary succession has recorded sequences covering duration of MIS-5 to MIS-1 and suggests a strong climatic control on the depositional environment. The glacial-interglacial cycles are in phase with the arid-humid cycles [Jain *et al.*, 2005; Kar *et al.*, 2001]. Humid phases are represented by gravel bed deposits (MIS-5 and 1) and reddening event (MIS-3). On the other hand, arid phases are represented by ephemeral sand-bed streams and aeolian deposits (MIS-2 and late MIS-3). Records from the Thar Desert and marginal areas exposed sequence of aeolian deposits covering past 200 ka. Wetter spell is recorded in the beginning of 200 ka followed by arid phase which shows extensive calcretes, sand dunes accumulation and playa formation [Dhir *et al.*, 1999, 2004]. Intense drying episodes are seen around 115 and 100 ka (colder sub-stages of MIS-5), 75 ka (MIS-4), and between 30-25 ka suggesting increase in aridity [Singhvi and

[Kar, 2004](#)]. Interesting finding by these authors is that during the LGM strong aridity was found in the Thar Desert, however aeolian activity was less. This is because even though the climate was arid, the of the strength summer monsoon wind responsible for dune building was weak and hence aeolian aggradation could not take place. This observation is also supported by studies carried out on marine sediment cores [[Sirocko et al., 1993](#)]. Intensification of monsoon is seen post LGM as stabilization of dunes and formation of paleosol layers during ‘climatic optimum’ (7-6 ka). Carbon isotopes in calcretes, soil and groundwater carbonates, derived from the Thar Desert sediments, have shown similar climatic fluctuations. C4 plants (grasses) were dominant during 70-60ka and 25ka (MIS-4 and 2) indicating weakened phase of monsoon, and their abundance reduced during enhanced phase of monsoon at around 60-25 ka, a time covering MIS-3 [[Andrews et al., 1998](#)]. Flood plain aggradation in Himalayan deposits at around 96-84 ka years (MIS-5) is an indicator of enhanced monsoon precipitation [[Sanyal and Sinha, 2010](#); [Suresh et al., 2007](#)]. Sediment core (Kalpi) along the Yamuna river channel and the Belan section, shows major floodplain aggradations in the Ganga plains during MIS 5 and 3. Relative dry phase of MIS-2 is seen as accumulation of aeolian and lacustrine deposits and by events of pedogenesis [[Gibling et al., 2005, 2008](#)]

5.1.1 The Kailash cave stalagmite

U-Th ages

$\delta^{18}O$ timeseries of Kailash cave samples is based on two U-Th ages shown in Table 5.1. Preliminary age model is constructed using ages of the top and bottom layers of the stalagmite. The sample was sent to the University of Taiwan for determining ^{230}Th ages for intermediate sampling intervals. Final age model will be constructed on procuring all the ages. However, timeseries based on a youngest and oldest ages, the sample growth is constrained between 13900 - 13400 yr BP

(Figure 5.2). The Kailash stalagmite grew at the rapid rate of ~ 1 mm/yr for ~ 500 years. The sample has several distinct growth bands, presumably annual in nature. The annual nature of the bands can be proved only after establishing the final chronology.

Stable isotopes of oxygen and carbon

The $\delta^{18}O$ values of the Kailash cave timeseries fluctuates between -3‰ to -0.5‰ from 13900 - 13450 years BP (Figure 5.3). A prominent ^{18}O depletion is observed post 13427 yr BP for only four years (13427 - 13423 yr BP) after which the sample growth had stopped. Repeat measurements were carried out for the same section twice and the analysis reproduced the same trend, hence the sudden ^{18}O depletion can not be treated as an artifact and indeed indicates a climate signal. A similar ^{13}C depletion is also observed in $\delta^{13}C$ record of the stalagmite, hinting at sudden change of climatic conditions. The record also shows periodic peaks of enriched ^{18}O values with corresponding enrichment in ^{13}C .

Table 5.1: Uranium and Thorium isotopic compositions and ^{230}Th ages of the subsamples of Kailash cave stalagmite. All errors are absolute 2σ values.

Sample	^{238}U (ppb)	^{232}Th (ppt)	$^{230}Th/^{232}Th$ activity ratio	$^{230}Th/^{238}U$ activity ratio	measured $\delta^{234}U$ (‰)	initial $\delta^{234}U$ (‰)	uncorrected age Yr BP	corrected age Yr BP
KLSH-1 (8.8mm)	151.82 ± 0.16	515.3 ± 3.8	0.16985 ± 0.00090	825 ± 7.5	451.0 ± 2.3	468.4 ± 2.4	13492 ± 79	13430 ± 85
KLSH-2 (530mm)	899.25 ± 0.99	2205.3 ± 8.8	0.17647 ± 0.00093	1186.5 ± 7.7	459.6 ± 2.4	478.0 ± 2.5	13960 ± 82	13916 ± 84

The degree of detrital ^{230}Th contamination is indicated by the $^{230}Th/^{232}Th$ atomic ratio instead of the activity ratio. Age corrections for samples were calculated using an estimated initial atomic $^{230}Th/^{232}Th$ ratio of 4 ± 4 ppm. Decay constants are $9.1705 \times 10^{-6} yr^{-1}$ for ^{230}Th , $2.8221 \times 10^{-6} yr^{-1}$ for ^{234}U [Cheng et al., 2013], and $1.55125 \times 10^{-10} yr^{-1}$ for ^{234}U [Mattinson, 2000].

Discussion

Although several studies focus on variability of ISM since the last deglaciation, the information is poorly resolved to address centennial climate variability of a particular event. The present study is intended to focus on decadal and centennial scale variability during 'Bolling-Allerod' event. Role of the North-Atlantic climate fluctuations effecting Indian ocean circulation and thereby influencing ISM was explained in the previous chapter.

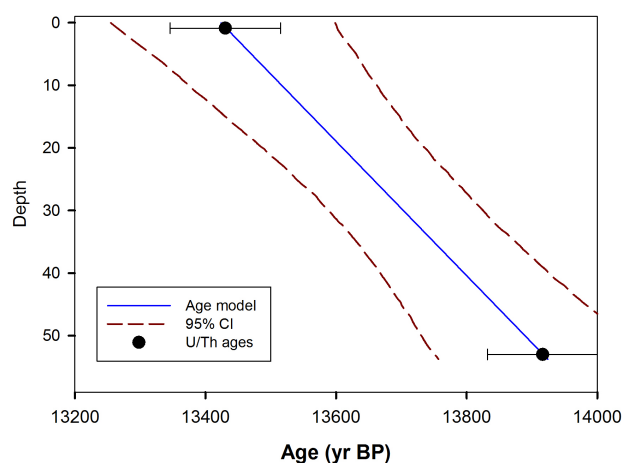


Figure 5.2: Age model of the Kailash stalagmite reconstructed using COPRA-interactive program on MATLAB [Breitenbach et al., 2012]. The filled black circles are ^{230}Th ages of topmost and bottom layers of the sample. The errors are reported in 2σ . The dashed lines show 95% confidence intervals and the blue line is the median through which the age model passes.

The sample growth is coincident with the warm and moist interstadial, known as 'Bolling-Allerod warming' in the last glacial period. Two stage oscillations are observed in this period. Bolling oscillation (peaked at 14.5 ka) and Allerod oscillation (peaked at 13 ka) were separated by older dryas. The $\delta^{18}\text{O}$ timeseries shows several fluctuations with prominent isotopic enrichment between 13.7 - 13.5 ka, indicating lower rainfall during older dryas. As in the Dandak and the Kotumsar caves, the $\delta^{13}\text{C}$ profile shows coeval changes with the $\delta^{18}\text{O}$ values implying that in extreme low precipitation conditions, even $\delta^{13}\text{C}$ values could

preserve a possible climate signal.

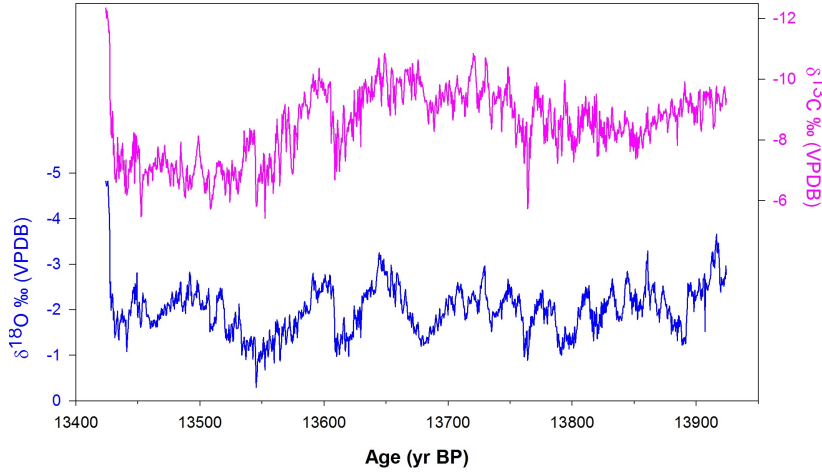


Figure 5.3: $\delta^{18}O$ and $\delta^{13}C$ timeseries of the Kailash cave stalagmite.

The abrupt depletion of $\delta^{18}O$ values at 13.3 ka followed by cessation of sample growth indicates higher precipitation coinciding with the peak of the Allerod oscillation. The sample deposition post this increase in rainfall stopped either due to the localized flooding at the sampling site or a high rate of drip water flow impeding calcite precipitation. A core raised from Bay of Bengal shows an increase in rainfall from 15.8 to 12.8 ka with concomitant increase in SST by 1.4°C [Govil and Naidu, 2011]. Kudrass *et al.* [2001]; Rashid *et al.* [2007] also observed that the Andaman Sea received more outflow from Irrawaddy river at 13.8 ka than at present. The increase in monsoon is also reported in Sanai Tal lake records from Ganga plains. The increase in monsoon around ~ 13 ka led to the expansion of lake and submergence of existing marshy lands [Sharma *et al.*, 2004].

Sinha *et al.* [2005] observed that $\delta^{18}O$ values of modern speleothem precipitate overlap with that of the deposits during the Bolling-Allerod event, implying that similar monsoon conditions prevailed during both the periods. The increase in rainfall during Bolling-Allerod is coincident with the increase in insolation after the last deglaciation. A speleothem record from the Timta cave [Sinha

et al., 2005], suggested a 60 years periodicity in ISM precipitation, during the late Bolling-early Allerod. Addressing such decadal variability in monsoon is possible only after a better chronological control is established for the sample.

5.1.2 The Belum cave stalagmite

The Belum cave receives an annual rainfall of 500 mm (Figure 5.4) of which 66% occurs during ISM (June to September) and 16% occurs during the withdrawing phase of the ISM (October). To understand the moisture sources contributing to the rainfall during the wet season (June to October), we carried out a Lagrangian back trajectory analysis using the HYSPLIT model [*Stein et al.*, 2015] with NCEP Reanalysis-1 [*Kalnay et al.*, 1996] as input to the model. We chose all the days with daily rain above 2 mm during 10 years (1998 to 2007 CE) for analysis. During ISM, trajectories suggest that the Arabian Sea is the major source of moisture, while during October, it is the mixture of the Arabian Sea and the Bay of Bengal (Figure 5.5). However, the major portion of annual rainfall is obtained from the Arabian Sea moisture, and the vapor reaching the cave is the remnant of the rainfall that occurred in the north-south oriented rainfall belt across the Western Ghats. Hence, the rainfall isotopic composition over the Belum cave is likely to reflect the rain out over the Western Ghat region. Since the actual measurement of rainfall isotopic composition from the cave is not available, we used the data from an isotope-enabled general circulation model, IsoGSM [*Yoshimura et al.*, 2008], in which the wind fields are constrained to observation (NCEP Reanalysis-2, *Kanamitsu et al.* [2002]) using the nudging technique. IsoGSM shows very good skill in predicting the spatio-temporal pattern of rainfall isotopic composition over ISM region on intra seasonal to inter-annual time scale [*Midhun and Ramesh*, 2015; *Midhun et al.*, 2016]. The inter-annual variation of the ISM rainfall $\delta^{18}O$ values at the Belum cave is well correlated with ISM rainfall over the Arabian Sea and Western Ghat region (Figure 5.6). This strengthens our hypothesis that the Belum rainfall isotopic composition is mainly controlled by the rainfall over

the Western Ghats and the Arabian Sea.

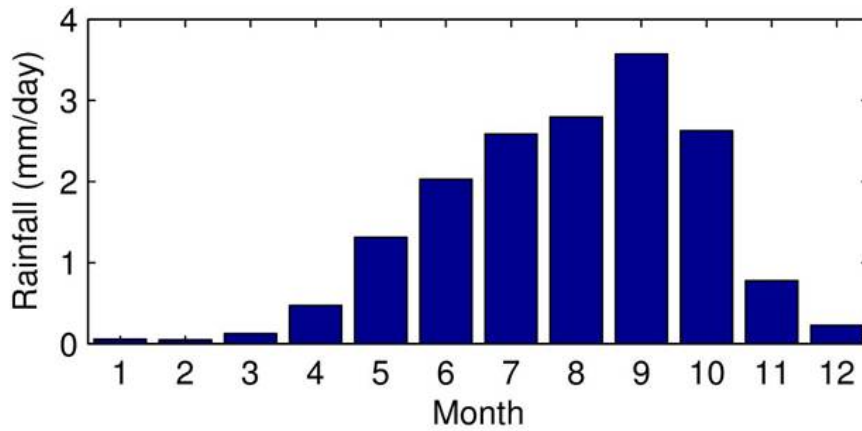


Figure 5.4: Climatological monthly rainfall at the 0.5×0.5 grid over the Belum cave. Climatology is calculated using Asian Precipitation - Highly-Resolved Observational Data Integration Towards Evaluation (APHRODITE) data from CE1951-2007 [Yatagai et al., 2012].

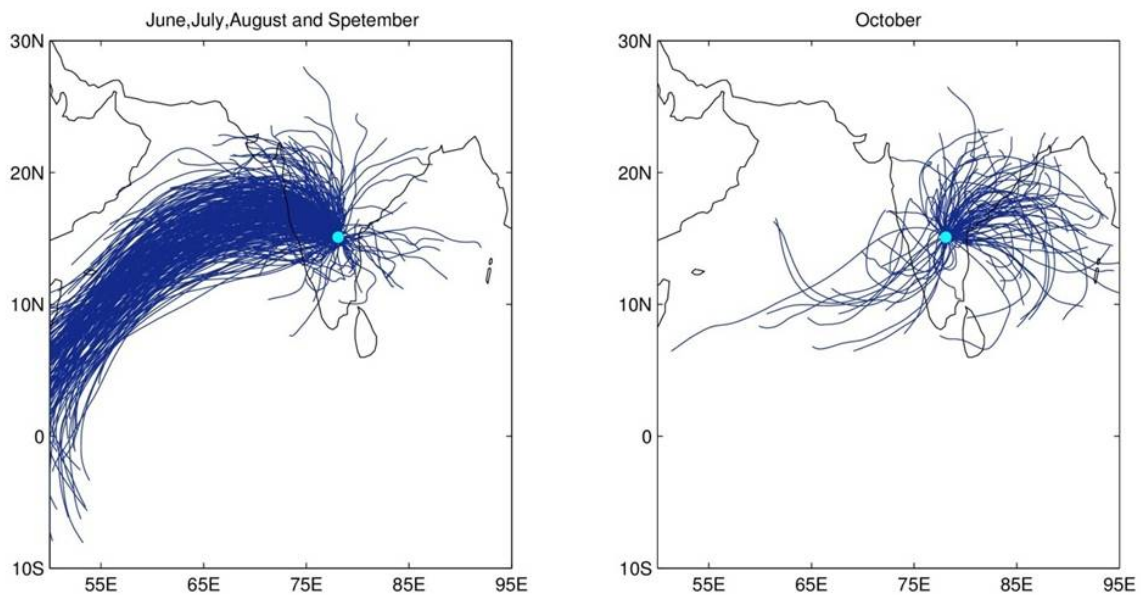


Figure 5.5: Three day back trajectory at 1500 m above ground level at the Belum cave calculated by the Hysplit [Stein et al., 2015] model using National Centre for Environmental Prediction (NCEP) reanalysis 1 dataset [Kalnay et al., 1996]. All days with rain above 2 mm during JJAS (left) and October (right) for ten years (1998-2007 CE) are used for analysis. Number of trajectories are 384 (JJAS) and 100 (October).

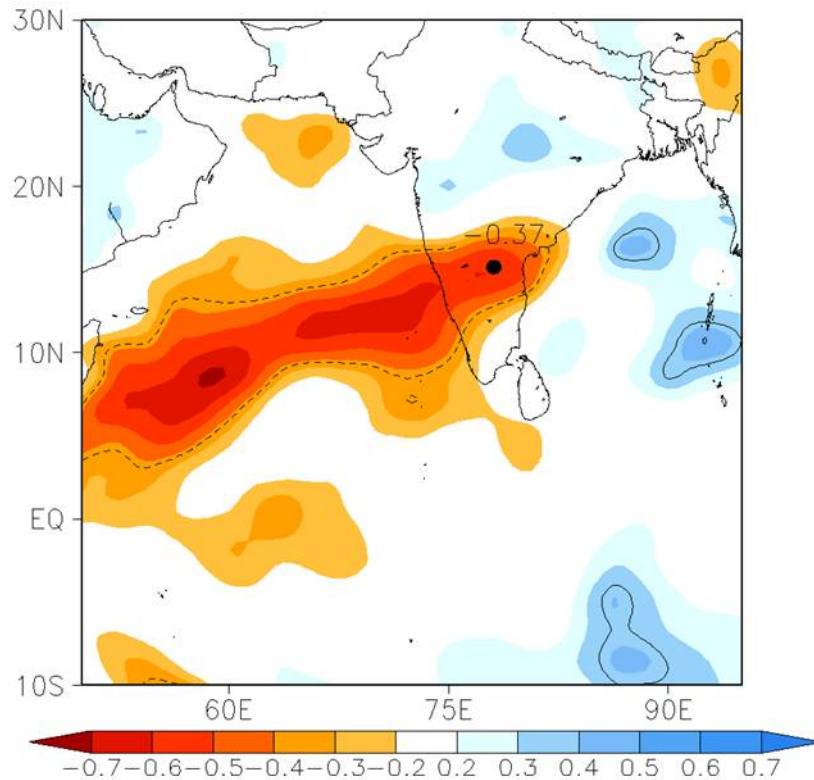


Figure 5.6: Correlation coefficient between model simulated JJAS average rainfall $\delta^{18}\text{O}$ at the Belum cave (Model resolution is $\sim 200 \times 200$ km) and model simulated JJAS average rainfall over surrounding grids, simulated by IsoGSM [Yoshimura et al., 2008]. Correlation with significance level $p = 0.05$ is marked by black dashed contour.

Minerology

The sample has three distinct growth zones representing the control of different climatic regimes. The lowermost section has white calcitic layers. The middle section has high detritus with porous radial crystals and the uppermost section has prominent growth layers. These three sections are separated by two hiatuses, one between the lower and the middle and the other between the middle and the uppermost sections (Figure 5.7), respectively. The hiatus is demarcated by a boundary of altered micro crystalline calcite with scattered inclusions of clay and Fe, evident in Figure 5.7.

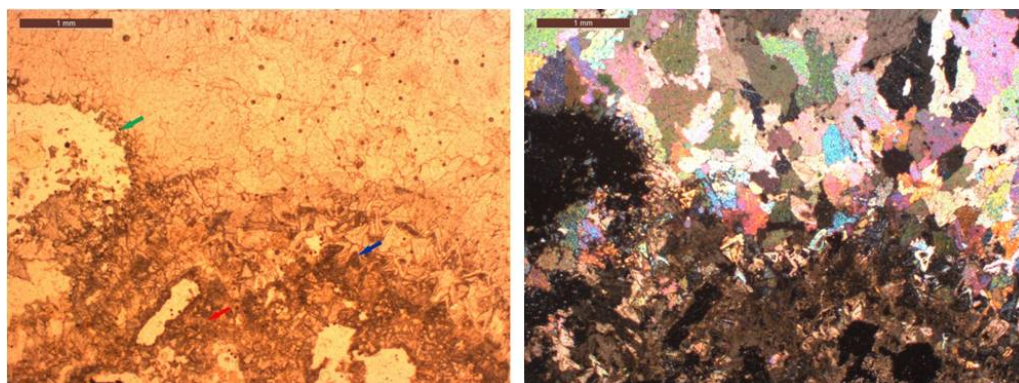


Figure 5.7: Photo taken under plane-polarized light (A) and cross-polarized light (B) shows a micro crystalline calcite layer (red arrow) below the hiatus boundary (green arrow). Calcite crystals along boundary show multiple growth zones (blue arrow) suggesting late stage precipitation. In the upper section of the photo euhedral crystals of calcite are seen post-hiatus. Micro photographs were taken using Leica DM EP microscope with attached Leica MC 120 HD camera at the M.S. University of Baroda, India.

U-Th ages

Sixteen ^{230}Th ages were obtained for the 31.4 cm long sample based on Th/U measurements (Table 5.2). The samples were analyzed by a Nu Instruments Multi-Collector Inductively Coupled Mass Spectrometer (MC-ICPMS) at the Oxford University, UK. Details of the instrument have been discussed in by *Belshaw et al.* [1998]. U concentrations were measured using a bracketing standard approach. Th was measured against in-house Th standards [*Mason and Henderson, 2010*]. Half-lives as calculated by *Cheng et al.* [2013] were used for calculations. The age data was further corrected for the presence of detrital Th using bulk detrital values of (5.38E-06, +5.38E-06, -4.84E-06) [*Hellstrom, 2006*]. From these ages, 10 subsamples have high U concentrations, for which the errors associated are less (Table-1 age). However, in the uppermost section of the sample, four ages show reversals due to low U content and relatively high ^{232}Th levels. As a result these ages are discarded. Since the Section 2 of the BLM-1 shows a high detrital content, only one age could be derived. Further dating of this section is difficult due to high ^{232}Th levels. The age model for the sample was constructed

using COPRA, an interactive age model [Breitenbach *et al.*, 2012]. A median age model with 2000 Monte-Carlo simulations and 95% confidence interval was derived. Since the section 2 is separated by two hiatuses at the top and bottom and has only one age, it was excluded from the age model. Sections 1 and 3 were modeled independently and merged together to establish a composite time series (Figure 5.8). Based on the age model, variable growth rates are observed in two sections. In section 1 growth rate increases from $1\mu\text{m}/\text{yr}$ to $5\mu\text{m}/\text{yr}$, whereas in section 3 the growth rate decreases steadily from $1\mu\text{m}/\text{yr}$ to $0.2\mu\text{m}/\text{yr}$.

Stable isotopes of oxygen and carbon

Temporal variations of $\delta^{18}\text{O}$ values are shown in Figure 5.9. The profile covers section 1 and 3 with an interval of, 183 to 173 ka and 104 to 81 ka, respectively. In section 1, the $\delta^{18}\text{O}$ values vary between -7.78‰ to -3.13‰ with an average of -4.74‰ (VPDB). In section 3, enrichment of 5‰ in ranging between -8.2‰ to -3.2‰ (VPDB) with abrupt changes was observed.

Trace element analysis

Trace element profiles of Mg/Ca, Sr/Ca, Ba/Ca and Mn/Ca are shown in Figure 5.10. Mg/Ca and Sr/Ca ratios have a good correlation ($n=101$, $r = 0.77$, significant at $p = 0.05$). All the three profiles follow the variations of the $\delta^{18}\text{O}$ trend. The major and trace element ratios increase abruptly between 85-90 ka.

Discussion

Both the sections of the sample preserve ISM variations during glacial periods, at 80-106 ka and 173-181 ka respectively. In the shorter timespan of section 1 (~ 8 ka) record, 2‰ enrichment was observed (Figure 5.9. The $\delta^{18}\text{O}$ values lie in the same range as that of the Section 3, implying both the glacial periods experienced weakening in monsoon intensity of a similar magnitude. The 5‰ stepwise enrichment in ^{18}O in section 3 during the last glacial inception can be attributed

to the declining intensity of monsoon. This, in addition with positive feedback factors such as increased evaporation from the overlying soil, could be responsible for the steep increase in $\delta^{18}\text{O}$. As a result, the infiltrating water is enriched in ^{18}O prior to precipitating in caves, and thus enhances the effect of less precipitation. The first step of 2‰ enrichment from -8‰ to -6‰ was observed from 106 – 98 ka, with a sharp increase in values at ~ 97 ka, subsequently followed by second step of 3‰ enrichment from -7 ‰ to -4‰. Interestingly, the second step is captured in the trace element record (Figure 5.10) as well. The concentrations of trace elements in speleothems depends upon various factors such as residence time in vadose zone, atmospheric dust input, temperature, and the amount of rainfall [Gascoyne, 1983; Verheyden, 2004; Verheyden et al., 2000]. However, the major climatic control of trace element concentrations in speleothems is the amount of rainfall [Verheyden, 2004]. Fairchild et al. [2000] suggested that Mg in speleothems can be used to reconstruct hydrological changes. Mg/Ca ratios are found to be sensitive to amount of rainfall and can be used in conjunction with stable isotope values to assess monsoon variability. Mg/Ca ratio in drip water is influenced by PCP and is higher during low-flow conditions. With the $\delta^{18}\text{O}$ values, the Mg/Ca and Sr/Ca ratios show negative correlations, implying higher ratios during drier conditions, favoring PCP [Cross et al., 2015]. Drier conditions prevailed during 90-85 ka, of MIS 5c seen as a sharp increase in the ratios. Mn is transported either as a organic complex, colloidal complex or as a particle in groundwater [Richter et al., 2004]. In the Belum cave stalagmite Mn could be associated with entrainment of colloidal particles adsorbed on mineral surfaces. Supporting evidence for this is seen as increased concentration of Mn where porous, impurity rich detrital layers are encountered and are significantly lower in the clear layers. Unlike what was observed by previous workers [Zhou et al., 2008], high Mn here content is not observed to be associated with an enhanced monsoon. On the contrary, it is seen when the precipitation was lower.

Table 5.2: Uranium and Thorium isotopic compositions and ^{230}Th ages of the subsamples of the Belum cave stalagmite. All errors are absolute 2σ values.

Sample	^{238}U (ppb)	^{232}Th (ppt)	$^{230}\text{Th}/^{232}\text{Th}$ activity ratio	$^{230}\text{Th}/^{238}\text{U}$ activity ratio	measured $\delta^{234}\text{U}$ (‰)	initial $\delta^{234}\text{U}$ (‰)	uncorrected age Yr BP	+	-	corrected age Yr BP	+	-
BLM-1 (2 mm)	271.51	8.85	5.19E-04	1.03	198.24	335.81	191359	1669	1668	190420	1776	1685
BLM-1R (2 mm)	306.99	9.75	5.27E-04	1.01	203.46	337.66	183613	2627	2460	182745	2587	2560
B1SN2 (2 mm)	271.8	9.47	-	1.01	198	331	183081	1998	1998	179557 †	2615	2615
BLM-3 (56 mm)	427.38	10.15	6.66E-04	0.97	172.04	281.60	178930	2087	1982	178222	2277	2076
BLM-4 (95 mm)	424.79	10.61	6.49E-04	0.98	184.30	301.11	178150	2070	2134	177420	2124	2129
BLM-5 (127 mm)	163.62	8.34	3.36E-04	1.04	231.64	383.05	182662	1336	1186	181294	1645	1780
BLM-6 (145 mm)	500.02	166.68	4.68E-05	0.95	203.26	305.16	157084	1044	1058	147201	8559	9734
BLM-7 (170 mm)	396.17	90.37	5.62E-05	0.78	197.50	261.67	109933	622	558	103250	5821	6390
BLM-8 (183 mm)	82.76	59.15	1.77E-05	0.77	220.96	276.02	104313	2765	2726	81441 §	20375	24614
BLM-9 (191 mm)	63.60	22.54	3.48E-05	0.75	230.73	293.36	98439	3013	2969	87304 §	10446	10660
BLM-10 (200 mm)	97.39	25.68	4.79E-05	0.77	235.99	326.06	99099	893	1030	91289 §	6795	7138
BLM-11 (214 mm)	63.91	12.21	6.34E-05	0.73	243.33	310.31	93879	3206	3127	882384 §	6057	5790
BLM-12 (228 mm)	174.28	6.76	3.35E-04	0.79	286.53	374.84	99028	521	591	98007	1112	1185
BLM-13 (250 mm)	278.18	5.53	6.00E-04	0.72	269.09	342.61	88665	442	562	88089	683	767
BLM-14 (280 mm)	464.44	16.634	3.25E-04	0.704	274.284	344.97	84991	671	653	84023	1216	1241
BLM-15 (305 mm)	272.01	13.62	2.29E-04	0.69	270.23	338.11	83534	820	769	821184	1563	1478
B1SN1 (305 mm)	256.80	7.14	-	0.68	270.0	340.00	82615	676	676	82009 †	737	737
BLM-16 (3125 mm)	478.55	383.38	1.45E-05	0.70	232.76	275.03	89634	640	570	61634	24809	286938

† ^{230}Th ages are discarded due to large errors. § ^{230}Th ages obtained from the University of New Mexico, New Mexico and verified by the ages obtained at the same sampling site. On comparison between ages of N2BLMS1 and N2BLMS10 with B1SN2 sampled at the same depth, N2BLMS10 was used in age model as it falls in the error limits of B1SN2. Half-lives as calculated by Cheng et al. [2013] were used for calculations. The age data was further corrected for the presence of detrital Th using bulk detrital value of ($5.38\text{E-}06$, $+5.38\text{E-}06$, $-4.84\text{E-}06$) [Hellstrom, 2006].

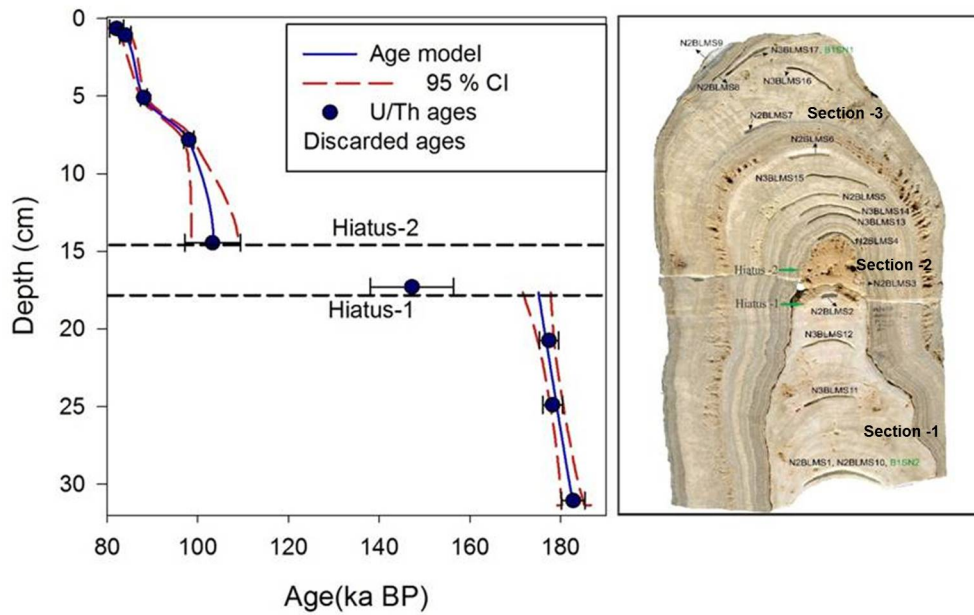


Figure 5.8: *Left: Age model reconstructed using COPRA- interactive program on MATLAB [Breitenbach et al., 2012]. The filled blue circles are ^{230}Th ages taken for age model. Two separate age models were constructed for sections younger and older than the hiatuses and then merged. The errors are reported as 2σ . The dashed lines show 95% confidence interval and the blue lines are the median through which the age model passes. Right: The Belum stalagmite is displayed against the age model. Sampling intervals for ^{230}Th ages are shown. Section 1 consists of white calcitic layers, towards the end of it the boundary is marked by a prolonged hiatus 1 (green arrow). Section 2 is composed of layers rich in detrital particles. And hence only one ^{230}Th age could be derived. Section 3, succeeds the former section by a brief hiatus 2 (green arrow), that covers last interglacial period.*

A possible explanation could be during enhanced monsoon, the drip rate is higher and the detrital particles accumulating at the tip of stalagmite are washed off. As a result, the calcium carbonate precipitating under high drip rate conditions has clear undisturbed growth layers. Study of seven stalagmites from the caves in Germany, show higher Mn concentrations in the autumn/winter sub annual layers. This enrichment is associated with enhanced weathering of soil cover during summer [Richter et al., 2004]. Section 3 covers the Marine isotope stages 5c to 5a. Surprisingly, there was no record of the interstadial 5e, the last inter-

glacial, during which the monsoon was stronger than the present [Burns *et al.*, 2001; Juyal *et al.*, 2006]. The lack of deposition during the last interglacial can be attributed to an enhanced monsoon which could have led to local flooding at the sampling site. The evidence of the erosional boundary are shown in the Figure 5.7. As described previously, the deeper chambers of the cave are at a lower elevation than the cave entrance, hence chances of flooding of these chambers are very high.

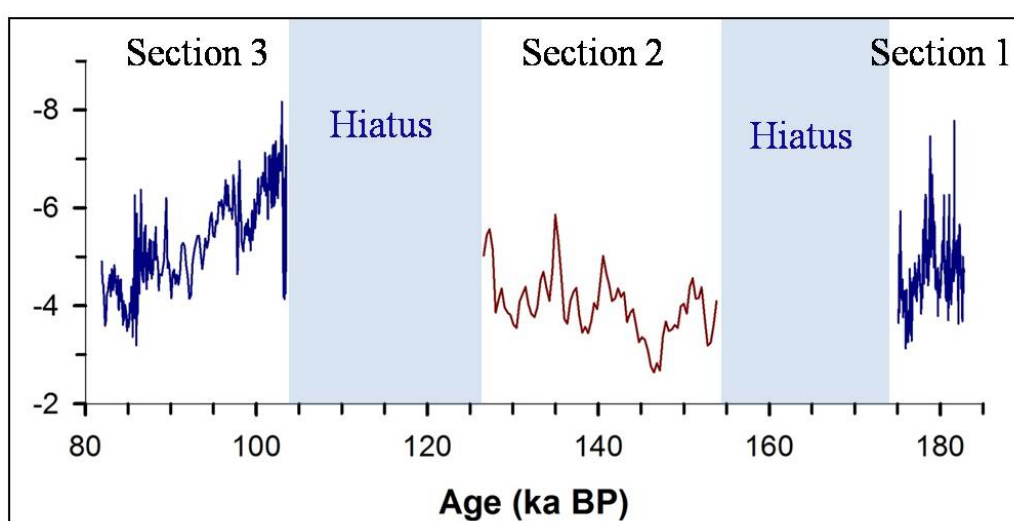


Figure 5.9: $\delta^{18}\text{O}$ profile of the Belum cave stalagmite. The blue curve represents the profile based on Copra age model. The red curve is a floating chronology based on a single U-Th date and is drawn to show the weaker monsoon phase prior to last interglacial, represented by hiatus (shaded region)

ISM has two sources for precipitation. The Arabian Sea component, ISMA mainly controls the rainfall over the Western Ghats and the region further east. And the Bay of Bengal component, ISMB, controls the rainfall over Northeastern India. Cai *et al.* [2015] presented a record from the Xiaobailong cave (XBL) located in southwestern china, representative of ISMB. Our record reflects on the ISMA branch more due to its major contribution to the sampling site (Figure 5.11). The $\delta^{18}\text{O}$ profiles of these two stalagmites from the the Belum and Xiaobailong cave representing two different sources, are comparable in the 104-80 ka timespan. Whatever could be the reason of variability during 173-180 ka, the climatic control

during last glaciation was same over both the regions.

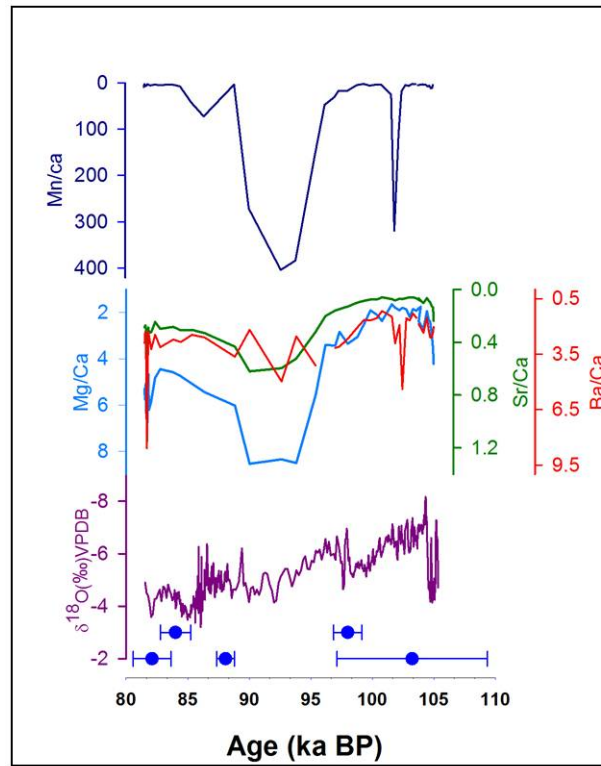


Figure 5.10: Comparison between the $\delta^{18}\text{O}$ profile of the Belum cave stalagmite (purple) and trace element ratios of Mg/Ca (light blue), Sr/Ca (green), Mn/Ca (dark blue) and Ba/Ca (red). Steep increase in ratios is seen between 90 to 85 ka, in the trace element ratios implying the role of PCP. ^{230}Th dates are shown as the blue filled circles with 2σ error bars.

Role of insolation gradient across the hemispheres in controlling monsoon

Intense heating of Indian subcontinent during the boreal summer leads to the formation of low pressure zone in north-northwestern India. As a result, there is a northward migration of the ITCZ, promoting southwesterly winds [Gadgil, 2003; Sikka and Gadgil, 1980]. The Indian monsoon system is unique in the sense that it occurs as a result of bi-hemispheric circulation. The pressure gradient between the Indian low over Central India and Mascarene high over southern Indian ocean is what drives the cross-equatorial transfer of heat [Webster et al., 1977; Zhisheng

et al., 2011]. The magnitude of this gradient determines the strength of the winds over India ocean [*Annamalai and Sperber*, 2016]. Earlier studies have shown that insolation has a direct impact on the intensity of monsoon (e.g., *Gupta et al.* [2005]). The $\delta^{18}O$ record of BLM-1 stalagmite was compared with the Northern Hemisphere insolation at 30°N. Our observation shows that there is an offset between the insolation and reconstructed monsoon profile. On the contrary the variability of the monsoon matches closely with the insolation gradient between the two hemispheres. A similar correlation was also seen in the Xiaobailong cave and the insolation gradient across the hemispheres (Figure 5.11 and 5.12). A likely explanation could be, that although insolation plays a key role in anchoring the low pressure zone over northwestern and central India, the circulation is controlled by the insolation gradient between the two hemispheres. Whenever this difference reduces the intensity of circulation reduces leading to a weaker monsoon.

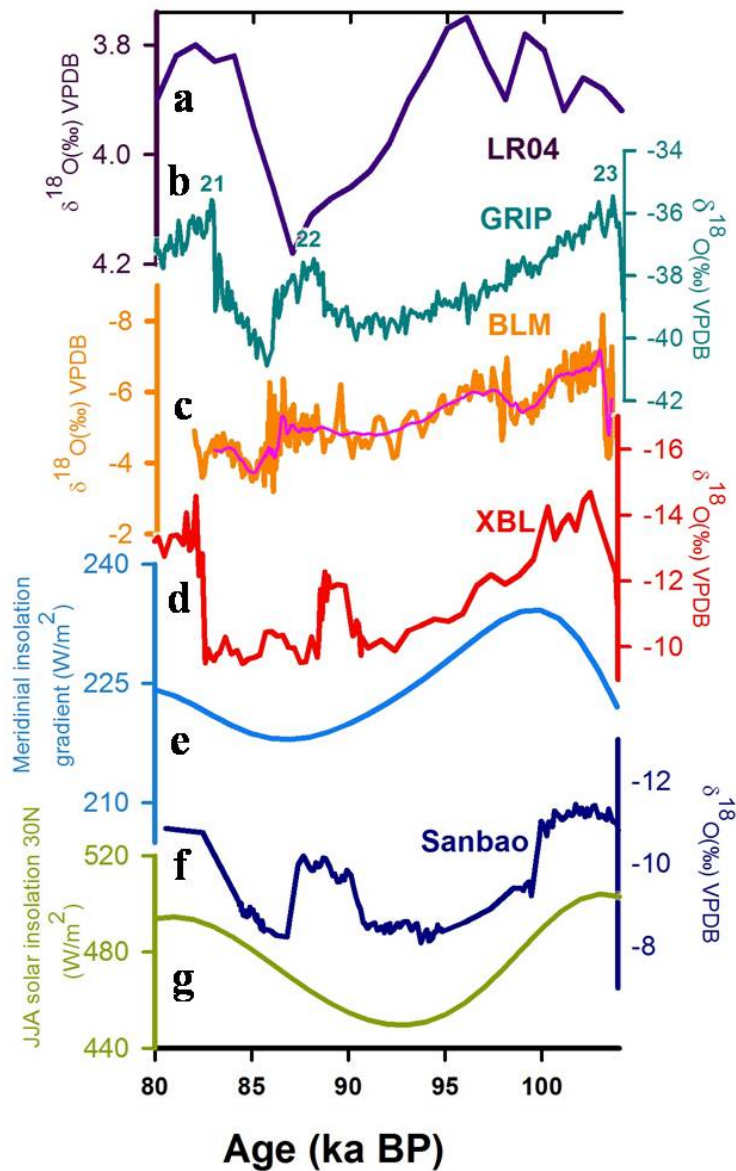


Figure 5.11: Comparison between (a) The LR04 benthic $\delta^{18}\text{O}$ stack (purple) constructed by graphic correlation of 57 globally distributed benthic $\delta^{18}\text{O}$ records [Lisiecki and Raymo, 2005] (b) fluctuations in $\delta^{18}\text{O}$ record of GRIP-2 (Greenland Ice Core Project, cyan) ice core from Greenland [Dansgaard et al., 1993; Grootes et al., 1993]. (c) The $\delta^{18}\text{O}$ values of stalagmite from the Belum cave (present study), India : BLM (orange). 25 year running average of the $\delta^{18}\text{O}$ records (pink). (d) The ISM record of a stalagmite from Xiaobailong cave: XBL (red) Cai et al. [2015] (e) meridional insolation gradient (light blue) between Northern and Southern latitudes at 30° N and 30° S [Berger, 1978; Berger A. and Loutre M.F., 1991] (f) $\delta^{18}\text{O}$ profile of a stalagmite from Sanbao cave (Blue, Wang et al. [2008]. (g) Northern Hemisphere 30° N solar insolation during JJAS.

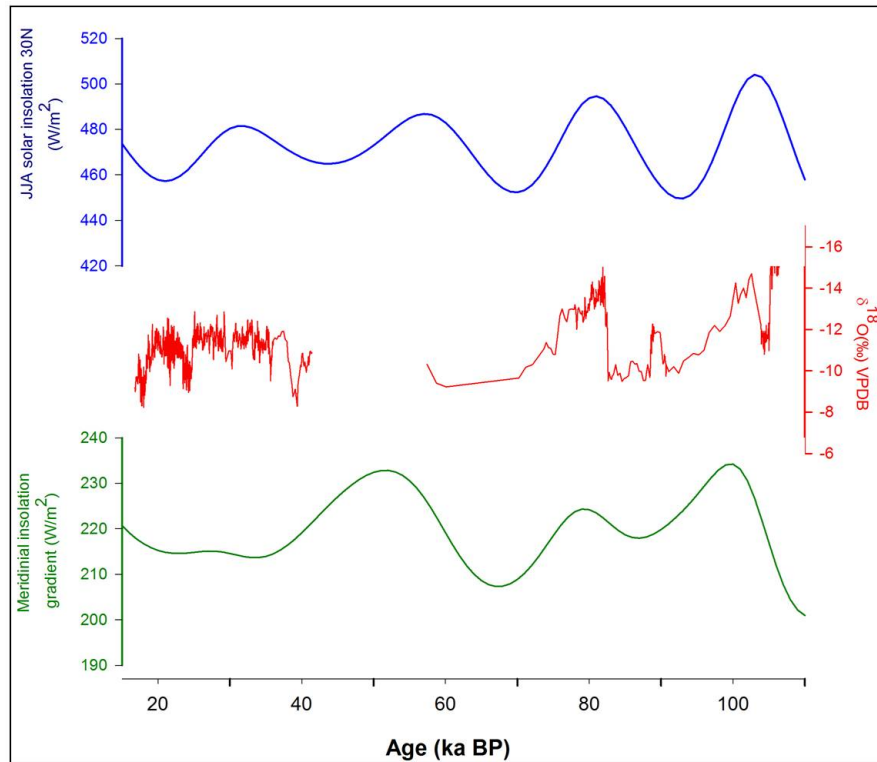


Figure 5.12: Comparison between long term composite records from the Xi-aobialong cave stalagmites (red) [Cai et al., 2015], with insolation at 30°N (blue) and inter-hemispheric insolation gradient (green) between Mascarene high over Indian ocean and tropical low over India [Berger, 1978; Berger A. and Loutre M.F., 1991].

5.2 Ocean monsoon record

Extensive work has been done on the Arabian Sea sediment cores recording monsoon variations of the past few thousand years. A complete monsoon record for the past 500 ka [Emeis et al., 1995] from a core (ODP site 723) raised near the Oman coast is in phase with major climatic boundaries. During colder phases of MIS 6, 4 and 2, abundance of *G. bulloides* was less, which in turn means a weaker upwelling and monsoonal winds in contrast to strong monsoonal winds, during MIS-5, 3 and 1. Figure 5.13 shows the locations of sediment cores from Arabian Sea and Bay of Bengal that have been investigated earlier. A detailed

study was carried out on core SO90-93KL from the Murray ridge, Arabian Sea. [Schulz et al. \[2002\]](#) studied the MIS-5/4 transition in detail. It was suggested that the well-known Toba volcanism in Indonesia that took place around 73 ka had not triggered the cooling during MIS-4, instead the climate had already begun cool prior to 73 ka. The $\delta^{18}O$ values of *G.ruber* fluctuated in accordance with Marine Isotopic Stages, with lower values during the interglacial and higher values during the glacial periods: during glacial periods much moisture from the ocean is locked into high latitudes in the form of ice which has lighter oxygen isotopic composition (i.e. more of $H_2^{16}O$ than $H_2^{18}O$ relative to ocean water), leading to less positive $\delta^{18}O$ values in ice sheets and hence more positive $\delta^{18}O$ values in the oceans, which is recorded by marine fauna. During interglacial periods, as glaciers start melting, the ocean becomes depleted in $H_2^{18}O$ and thus more negative $\delta^{18}O$ values are recorded by marine microfossils during interglacial periods. In response to such changes, lower values are observed during MIS 5, 3 and the lowest at MIS-1 (Last Glacial Maximum LGM, 21 ka). Another core from the Murray ridge (Site - NIOP4, [Reichart et al. \[1997\]](#)) covers a time span of ~ 225 ka, where $\delta^{18}O$ of *Neogloboquadrina dutertrei* was used to reconstruct climate. It is seen that during the warmer periods MIS-5, 3 and 1, primary productivity and the abundance of *G.bulloides* were in phase with strong monsoonal conditions. Sediments deposited in the Bay of Bengal by major rivers, e.g. the Ganga-Brahmaputra, and their amount varies in response to monsoon performance. [Kudrass et al. \[2001\]](#), using a core raised (SO93-126KL) from the northern Bay of Bengal, have addressed monsoon variability during past 80 ka. Here the monsoon signal is recorded as more negative $\delta^{18}O$ values corresponding to higher monsoon run-off from the Indian rivers. In this record, LGM is characterized by the highest values of $\delta^{18}O$, indicating that the freshwater flow was significantly reduced during this period. This is followed by rapid decrease in the $\delta^{18}O$ values associated with global melt water infusion and increase in sea level. Our record focuses on ISM variability from MIS-3 to 1 and is discussed below.

5.2.1 The Andaman Sea sediment core

Schulz et al. [1998] observed a correlation between the Indian Monsoon and Greenland climate oscillations on glacial-interglacial timescales. The last Glacial period (110 - 10 ka) witnessed millennial scale climate variability in terms of abrupt transitions between several cold stadials and warm interstadials. Many of these stadials were interrupted by ice-rafting events known as 'Heinrich Events'. Seven such events have been reported in the last glacial period. Climate variability associated with these cold events is not restricted to North-Atlantic basin, instead it is observed in low latitudes as well, due to rapid changes in atmospheric and ocean circulations [*Pausata et al.*, 2011].

The present study is focused on the understanding the response of the Northern Indian Ocean to such climate events and reconstruct the ISM during the last 200 ka. The objective was achieved using a core SK-234-60 raised from Andaman Sea and the Belum stalagmite (discussed in section 5.1.2) and a review of the available literature. *Awasthi et al.* [2014], identified three sources of sedimentation to the Andaman Sea: (1) the Irrawaddy catchment, (2) the western slopes of the Indo-Burman-Arakan (IBA) mountain ranges and the Andaman Islands, and (3) the catchments of Salween and Sittang and the Bay of Bengal shelf. Around 30-60% of the sediments are derived from the first two sources. The sediment flux associated with these sources depends upon the intensity of rainfall and reach their peak during the monsoon season around July-August [*Rashid et al.*, 2007].

Awasthi et al. [2014], reported the highest rate of sedimentation of 8.4 cm/ka during 52.0 – 57.5 ka and the lowest of ~ 2.4 cm/ka during the LGM, i.e., at 17.3 – 23.5 ka. The average sedimentation rate in the core was estimated to be 5.6 cm/ka. Sedimentation rate during MIS-3 was 5.5 cm/ka, followed by decreased rate of 3.0 cm/ka during the MIS-2 and rapid increase in rate of 7.7 cm/ka during the MIS-1 (Holocene).

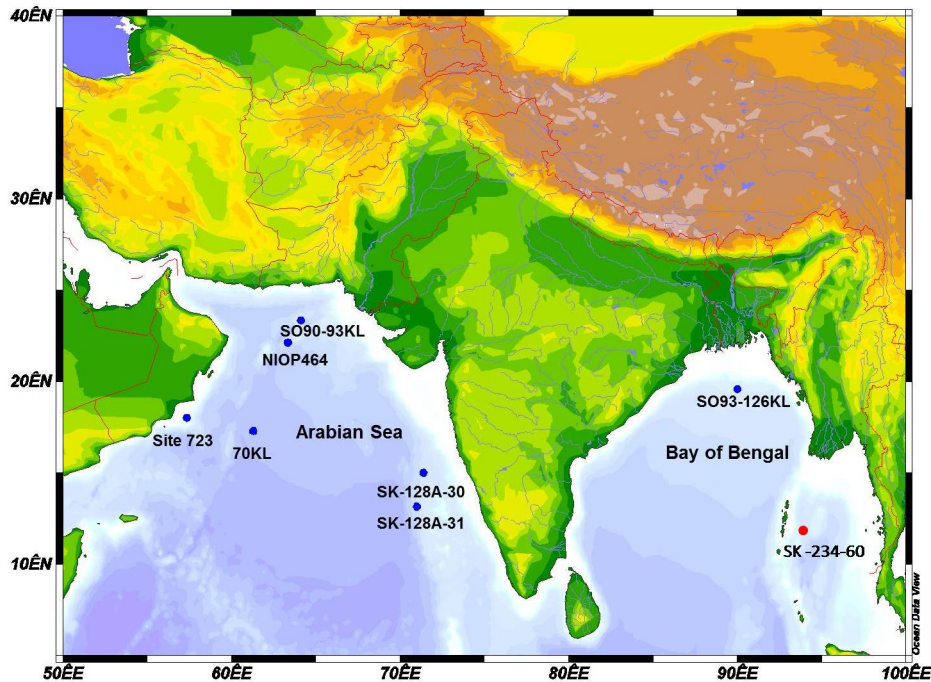


Figure 5.13: Locations of different cores raised from the Arabian Sea and the Bay of Bengal. (Site 723, *Emeis et al. [1995]*), (Site: SO90-93KL, *Schulz et al. [2002]*), (Site: NIOP464, *Reichart et al. [1997]*), (Site: SO93-126KL, *Kudrass et al. [2001]*), (Site: 70KL, *Leuschner and Sirocko [2000]*), (Site: SK-128A-30 and SK-128A-31, *Prabhu et al. [2004]*, Site: SK-234-60, present study (red).

Based on the geochemical properties and hence the provenance of the sediments, *Awasthi et al. [2014]* concluded that the strength of the Indian Summer Monsoon (ISM) over western Myanmar and Andamans during the Last Glacial Maximum (LGM) was similar to the present. However, the provenance of the sedimentation can give little information about the strength of the monsoon. After reanalysis of the $\delta^{18}O$ values of *G. ruber* of the present core and comparing the record with pteropod abundances from core SK 168/GC1, a weaker ISM during the LGM is inferred. *Sijinkumar et al. [2010]* interpreted the late Quaternary climate using the abundance of pteropods in the Andaman sediment core SK 168/GC1. They observed high abundances on account of better preservation during the LGM, while lower abundance of pteropods throughout the Holocene.

Most importantly they reported high abundance of mesopelagic pteropods as

compared to epipelagic species, explaining deep water mixing, weaker Oxygen Minimum zone (OMZ) and lower Aragonite Compensation Depth (ACD). During LGM, weakening of summer monsoon reduced the ocean stratification by low influx of fresh water and strengthening of winter monsoon resulted in vertical mixing, increasing ACD favoring the pteropod preservation [Sijinkumar *et al.*, 2010]. Sarkar *et al.* [1990]; Sijinkumar *et al.* [2011] and Duplessy [1982] also pointed out that during LGM summer monsoon was weaker and there was strengthening in winter monsoon. Another study from the Andaman Sea [Rashid *et al.*, 2007] also reported a weaker summer monsoon during the LGM. Based on these evidences, we infer that the geochemical signatures of IBA as provenance during LGM to Andaman Sea reported by Awasthi *et al.* [2014] are not due to the strengthening of the summer monsoon over western Myanmar. Instead, the bulk load of sediments were transported and deposited at the core site owing to a stronger winter monsoon.

Based on Mg/Ca, Rashid *et al.* [2007], postulated that the Andaman Sea was cooler at LGM in comparison to late Holocene by 3°C. Similar cooling is also observed in the tropical Indian ocean by Bard *et al.* [1997]; Naidu and Malmgren [2005] and in the Bay of Bengal by Kudrass *et al.* [2001]. Further, Rashid *et al.* [2007] argues that late-glacial period (19-14.8 ka) was the phase of the weakest monsoon in the past 25 ka. Our records shows that LGM (25-19 ka) was the weakest monsoon period in the last 70 ka.

Existing records from the Bay of Bengal and the Andaman Sea show a strong relation between the Greenland climate oscillations and ISM variability. Most of these studies focus on migration of Ganga-Brahmaputra delta at water depths which are closer to sea level to a few tens of meters [Goodbred, 2003; Goodbred and Kuehl, 2000; Rashid *et al.*, 2007].

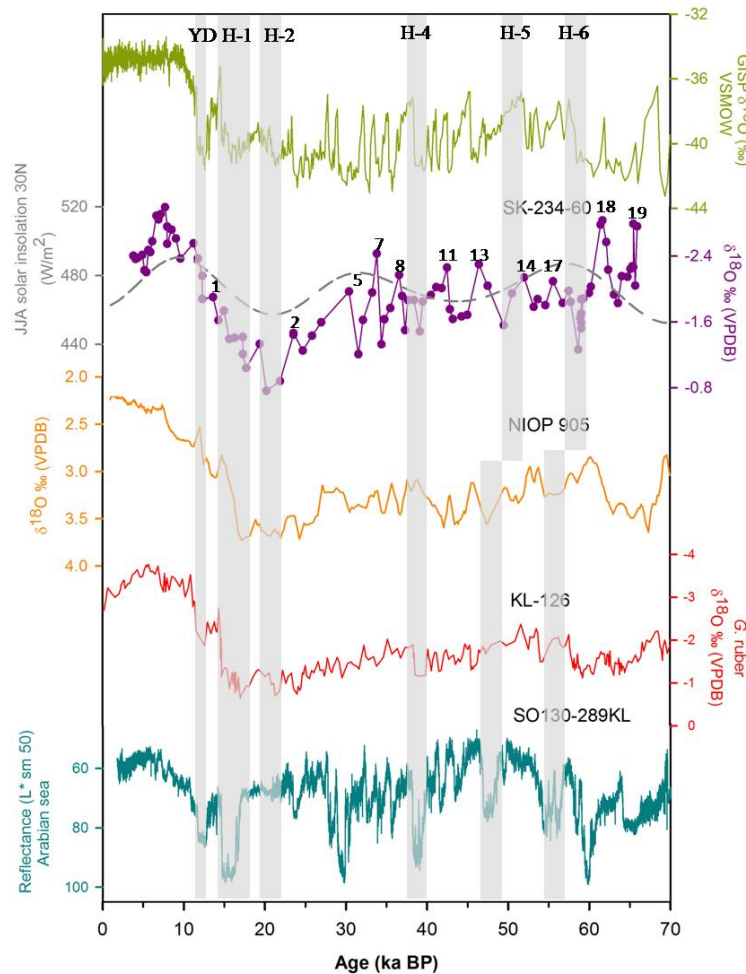


Figure 5.14: Comparison of $\delta^{18}\text{O}$ values of GRIP ice core (Green, [Grootes and Stuiver \[1997\]](#)), $\delta^{18}\text{O}$ timeseries of Andaman Sea sediment core SK (present study), the dashed gray line shows insolation at 30°N , the $\delta^{18}\text{O}$ record of the planktic foraminifera *N. dutertrei* from the Arabian Sea sediment core NIOP-905 (Yellow, [Jung et al. \[2009\]](#)), $\delta^{18}\text{O}$ values of a core from the Bay of Bengal (Red, [Kudrass et al. \[2001\]](#)) and the reflectance data from the Arabian Sea sediment core SO130-289KL, (Cyan, [Deplazes et al. \[2013\]](#)) The gray vertical bands represent ice calving events in the North-Atlantic known as Heinrich events and are shown from H-1 to H-6, the colder stadial Younger Dryas is shown as YD. The recorded Daansgard-Oeschger events are numbered from 1 to 19.

[Colin et al. \[1998, 1999\]](#), based on high magnetic susceptibility and increase in smectite/(illite+chlorite) ratio and $^{87}\text{Sr}/^{86}\text{Sr}$ in sediment cores raised from the Andaman Sea and Bay of Bengal showed increase in ISM during the Bolling-Allerod and the Daansgard-Oeschger events. Our record, within the age un-

certainty responds to Heinrich events by showing prominent enrichment in ^{18}O values, as shown in figure 5.14. Ice calving episodes recorded in the North-Atlantic, disrupt the ocean circulation; as a result, the Indian Ocean became more enriched during these events. The $\delta^{18}\text{O}$ profile of the present study shows coeval changes with $\delta^{18}\text{O}$ values of the sediment cores raised from the Bay of Bengal (NIOP 905) and the Arabian Sea (KL-126) implying that the records preserves changes in the Indian Ocean circulation. Moreover, the $\delta^{18}\text{O}$ timeseries is based on Dansgaard-Oeschger events (beyond the limit of radiocarbon dating) signifying the role of North-Atlantic climate changes in controlling the Indian ocean circulation, including the water currents passing through the Preparis channel. During the LGM the south Preparis current was active in spite of lowering of mean sea level by 120 m, bringing the waters enriched in ^{18}O from the Bay of Bengal. The troughs in our data correspond to the cooling events in Greenland ice core records as seen in figure 5.14.